ACS OMEGA

http://pubs.acs.org/journal/acsodf

Review

Pedagogical Overview of the Fewest Switches Surface Hopping Method

Amber Jain* and Aarti Sindhu

Cite This: *ACS Omega* 2022, 7, 45810−45824

Read Online

ACCESS | Metrics & More | Article Recommendations

ABSTRACT: The fewest switches surface hopping method continues to grow in popularity to capture electronic nonadiabaticity and quantum nuclear effects due to its simplicity and accuracy. Knowing the basics of the method is essential for the correct implementation and interpretation of results. This review covers the fundamentals of the fewest switches surface hopping method with a detailed discussion of the nuances such as decoherence schemes and frustrated hops and the correct approach to calculating populations. The consequences of incorrect implementation are further discussed toward calculating kinetic and thermodynamic properties. Some tips for practitioners and a step-by-step algorithm for developers are provided. Finally, some of the finer technicalities of the fewest switches surface hopping method that are buried deep in the literature are pointed out to help graduate students better appreciate this method.

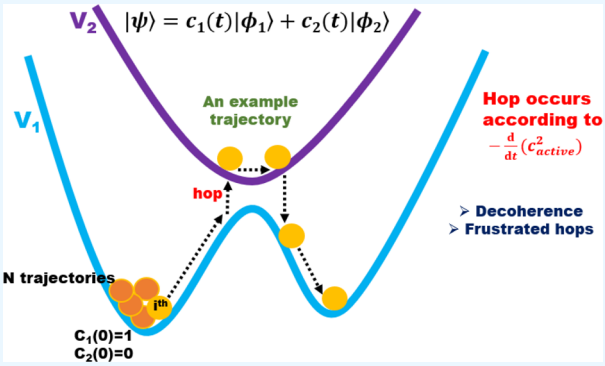

1. INTRODUCTION

The fewest switches surface hopping (FSSH)[1] method is one of the most used methods for nonadiabatic dynamics.[2−10] Several packages are now available that can integrate with electronic structure packages to run FSSH simulations on the fly, such as SHARC,[11] JADE,[12] NewtonX,[13] PYXIAD,[14] Libra,[15] ANT,[16] and Q-Chem.[17] A correct usage of this method is necessary to obtain meaningful insights. For example, if decoherence or frustrated hops are not treated correctly, one might get qualitatively wrong reaction dynamics or thermal properties.

This review is meant to be a pedagogical text to expose the basic ideas of the surface hopping method to those who are beginning to get into this field. We have included the basic derivations, with some tricks of the trade that are well-accepted practices in the surface-hopping community but are scattered in the literature.

For the FSSH methodology practitioners, this review provides intuition and tips for choosing the correct details for running the simulations and correctly interpreting the results. For those who wish to code this method themselves, this review provides some finer nuances that are hard to find in the literature but essential to the method with a detailed algorithm.

With this review, a basic open-source code in Python for FSSH is provided in ref 18. Further, a Python code to perform numerically exact quantum dynamics for a 2-level system interacting with one nuclear coordinate is provided in ref 19. We encourage the students reading this review to use these codes to compare the populations and coherences for low-dimensional model problems calculated from surface hopping and exact quantum dynamics. This should help build intuition for the correct treatment of decoherence and frustrated hops, which are critical components in FSSH.

This review is organized as follows: Section 2 introduces the Born−Oppenheimer setup, followed by an introduction to FSSH in Section 3. The decoherence issue is described in Section 4; a correct interpretation of the FSSH method to calculate diabatic populations is described in Section 5; and a discussion of frustrated hops is given in Section 6. Consequences of decoherence and frustrated hops to the thermal properties are discussed in Section 7, and the vibrational nonadiabaticity is discussed in Section 8. Some of the nuances in coding the FSSH method are given in Section 9, followed by some tips for practical usage of surface hopping in Section 10. The codes can be found in Section 11, some of the challenges and opportunities in Section 12, and conclusions in Section 13.

Received: July 31, 2022
Accepted: November 18, 2022
Published: December 8, 2022

2. BORN−OPPENHEIMER SETUP

We first introduce the Born−Oppenheimer setup to define our notation. The system's degrees of freedom are partitioned into "fast" modes q and "slow" modes R. In general, q and R are vectors representing the coordinates of the corresponding degrees of freedom. For clarity of notation, we are not using vector signs throughout the review.

Usually, q are the electronic coordinates, and R are the nuclear coordinates. However, there is no such requirement. We can also include some nuclear modes in the "fast" degrees of freedom q.

The total Hamiltonian of the system is given as

$$H = \hat{T}_R + H_{\mathrm{el}} \tag{1}$$

$$H_{\mathrm{el}} = \hat{T}_q + V(q, R) \tag{2}$$

where $\hat{T}_R$ and $\hat{T}_q$ are the kinetic energy operators for the R and q modes, respectively, and $V(q, R)$ is the total potential energy.

Given that R are the slow modes, it is natural to form a complete basis for the total system as the eigenfunctions of H_{el} at fixed configuration R:

$$H_{\mathrm{el}}\phi_i^{\mathrm{ad}}(q, R) = E_i^{\mathrm{ad}}(R)\phi_i^{\mathrm{ad}}(q, R) \tag{3}$$

We will refer to these solutions, E_i^{ad} and ϕ_i^{ad}, as adiabatic eigenenergies and adiabatic eigenfunctions, respectively. The complete wave function of the system can now be written as

$$\Psi(q, R, t) = \sum_i \chi_i(R, t)\phi_i^{\mathrm{ad}}(q, R) \tag{4}$$

We emphasize that eq 4 is an exact quantum mechanical expression. At each R, $\phi_i^{\mathrm{ad}}(q, R)$ is a complete set in q space. Therefore, the exact wave function can be expanded in this adiabatic basis at that R. For different R, the coefficients will be different and given by $\chi_i(R, t)$. The expansion in eq 4 is true, however, only if the summation is not truncated and $\chi_i(R, t)$ is calculated without any further approximations, which for real systems might not be numerically possible.

It is often the case that one is interested only in the q subsystem. The subsystems (q or R) cannot be described in general by a wave function. Instead, a complete description of the subsystem is given by a reduced density matrix

$$\rho_{\mathrm{el}}(t) = Tr_R\rho(t) \tag{5}$$

where Tr_R is the trace over the R coordinates, and ρ is the total $(q + R)$ density matrix: $\rho(t) = |\Psi(t)\rangle\langle\Psi(t)|$.

3. ALGORITHM OF THE FEWEST SWITCHES SURFACE HOPPING METHOD

FSSH is a mixed quantum-classical method that considers the slow modes R classically and the fast modes q quantum mechanically. It is a trajectory-based stochastic method to calculate approximately $(R(t), \rho_{\mathrm{el}}(t))$. Further, in this method, the trajectories are independent, allowing for fast parallelization of codes.

We start with a summary of the basic FSSH algorithm described by Tully in ref 1. In the FSSH method, the classical subsystem is described by the phase space $(R(t), P(t))$, where P are the momenta, and the quantum subsystem is described by a wave function $\psi_{\mathrm{el}}(q, t)$. As discussed in the previous section, the quantum subsystem is correctly described by a reduced density matrix (eq 5). In general, the total wave function might not be separable into an electronic and a nuclear wave function, and assigning an electronic wave function is an ansatz.

The electronic wave function is expanded in a complete basis as

$$\psi_{\mathrm{el}}(q, t) = \sum_j c_j(t)\phi_j(q, R(t)) \tag{6}$$

We refer to $\phi_j(q, R(t))$ as a diabatic basis, and this basis is the choice of the user. It often depends on the problem under investigation: for example, these might be the bright states when investigating absorption spectroscopy.

The potential energy surfaces for the classical subsystem are assumed to come only from one of the diagonal matrix elements of the electronic Hamiltonian: $V_{\lambda\lambda}(R) = \langle\phi_\lambda(R)|H_{\mathrm{el}}|\phi_\lambda(R)\rangle$ (where the integration is done over the q coordinates). λ will be used to denote the active surface from now on. With this, the evolution of the classical subsystem is given by

$$m\ddot{R} = -\nabla_R\langle\phi_\lambda(R(t))|H_{\mathrm{el}}|\phi_\lambda(R(t))\rangle \tag{7}$$

Assuming that $\psi_{\mathrm{el}}(q, t)$ obeys the time-dependent Schrödinger equation

$$i\hbar\dot{\psi}_{\mathrm{el}}(q, t) = H_{\mathrm{el}}\psi(q, t) \tag{8}$$

and substituting eq 6 in eq 8 gives

$$i\hbar\sum_j [\dot{c}_j(t)\phi_j(q, R(t)) + c_j(t)\dot{\phi}_j(q, R(t))] = \sum_j c_j(t)H_{\mathrm{el}}\phi_j(q, R(t)) \tag{9}$$

Multiplying with $\phi_k^*(q, R(t))$ and integrating over q gives

$$i\hbar\dot{c}_k(t) = \sum_j (V_{kj}(R(t)) - i\hbar T_{kj})c_j(t) \tag{10}$$

where $V_{kj}(R) = \langle\phi_k(R)|H_{\mathrm{el}}|\phi_j(R)\rangle$ and $T_{kj} = \left\langle\phi_k(R(t))\middle|\frac{d}{dt}\phi_j(R(t))\right\rangle$ is the time-derivative nonadiabatic coupling matrix. One useful relation to note is $T_{kj} = v\cdot d_{kj}$, where $d_{kj}(R) = \left\langle\phi_k(R)\middle|\frac{d}{dR}\phi_j(R)\right\rangle$ is the derivative coupling vector (often called the nonadiabatic coupling (NAC)), and v is the velocity.

Finally, to account for nonadiabaticity, the active surface λ can change depending on the rate of change of $|c_\lambda|^2$. Using eq 10, it is easy to show

$$-\frac{d|c_\lambda|^2}{dt} = \sum_k \left(2Re(T_{\lambda k}c_\lambda^* c_k) - \frac{2}{\hbar}\mathrm{Im}(V_{k\lambda}c_\lambda^* c_k)\right) \tag{11}$$

Each term in the summation in eq 11 is interpreted as the rate of population transfer from state λ to state k, given by $\left(2Re(T_{\lambda k}c_\lambda^* c_k) - \frac{2}{\hbar}\mathrm{Im}(V_{k\lambda}c_\lambda^* c_k)\right)$. Using a time step dt much smaller than the time scale of hopping, the hopping probability during the time interval dt from state λ to state k then is proportional to $\left(2Re(T_{\lambda k}c_\lambda^* c_k) - \frac{2}{\hbar}\mathrm{Im}(V_{k\lambda}c_\lambda^* c_k)\right)dt$. Normalizing with the current population in state λ gives the final hopping probability as

https://doi.org/10.1021/acsomega.2c04843
ACS Omega 2022, 7, 45810−45824

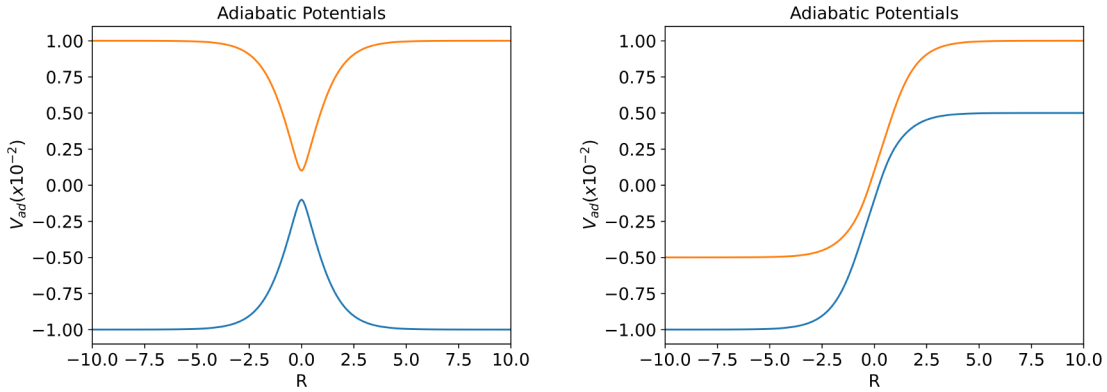

Figure 1. Two model adiabatic potential energy surfaces of eq 13. (a) Nonparallel potential energy surfaces with $A_2 = -0.01$ and (b) nearly parallel potential energy surfaces with $A_2 = 0.005$. All numbers are in atomic units.

$$g_{\lambda\to k} = \frac{2Re(T_{\lambda k}c_\lambda^* c_k) - \frac{2}{\hbar}\mathrm{Im}(V_{k\lambda}c_\lambda^* c_k)}{|c_\lambda|^2}dt \tag{12}$$

Notice that the hopping probability in eq 12 can be negative. That would signify a hop from state k to state λ. In the spirit of the fewest hops, these hops with negative hopping probability are ignored.

As a concrete and a simplified example, consider that at some time t there are 80 trajectories on state 1 and 20 trajectories on state 2, with $|c_1|^2 = 0.8$ and $|c_2|^2 = 0.2$. After a small time step dt, say the quantum coefficients change such that $|c_1|^2 = 0.7$ and $|c_2|^2 = 0.3$. Therefore, $(0.8-0.7)/0.8 \times 80 = 10$ trajectories should hop from state 1 to state 2, and no trajectory should hop from state 2 to state 1 to achieve the desired result of 70 trajectories on state 1 and 30 trajectories on state 2.

It is common to use the adiabatic basis $\phi_j^{\mathrm{ad}}(q, R)$ of eq 3 to perform the FSSH simulations. In this case, $V_{jk}(R) = E_j^{\mathrm{ad}}(R)\delta_{jk}$, and the forces can be calculated using the Hellman−Feynman theorem $m\ddot{R} = -\langle\phi_\lambda^{\mathrm{ad}}(R(t))|\nabla_R H_{\mathrm{el}}|\phi_\lambda^{\mathrm{ad}}(R(t))\rangle$. The hopping probability in the adiabatic basis simplifies to $g_{\lambda\to k} = \frac{2Re(T_{\lambda k}c_\lambda^* c_k)}{|c_\lambda|^2}dt$.

Now a few points are worth noting:

- The state of the system in FSSH for each trajectory is defined by classical phase space (R, P), state of the system λ, and quantum amplitudes c_j.
- FSSH is a stochastic method with independent trajectories. The hopping probabilities depend solely on the current state of the system.
- The wave function ψ_{el} only obtains the hopping probability. **It should not be interpreted as the wave function of the quantum system.** See Section 5 for a discussion. The rate of change of $|c_\lambda|^2$ is a good indicator of the rate of change in the population of the state λ; however, $|c_\lambda|^2$ itself might be a bad indicator of the population of the state λ.[20,21]
- On a hop, velocity has to be adjusted to conserve energy. This adjustment is typically performed along the direction of the nonadiabatic coupling vector $d_{\lambda k}$ (for a hop occurring from state λ to state k). More discussion on this can be found in Section 6.

4. DECOHERENCE

FSSH is usually an overcoherent method. We first discuss the origins of coherence and decoherence from exact quantum dynamics compared with FSSH dynamics, followed by the consequences of not including decoherence and different approaches to include decoherence.

4.1. Fundamentals of Coherence. To understand coherences, we investigate two simple model systems, having two electronic states and one nuclear degree of freedom R. We have so far been describing electronic coordinates using the symbol q. We now move to a diabatic basis description which is more convenient. This diabatic basis we define as any complete basis in the electronic space, such as $\phi_j(q, R(t))$ used in the previous section (see eq 6). For convenience, we will drop the q and R terms and write the diabatic basis using the notation $|j\rangle$.

In a diabatic basis, we consider a Hamiltonian of the form

$$H = \frac{p^2}{2m} + \begin{pmatrix} A_1\tanh(BR) & Ce^{-DR^2} \\ Ce^{-DR^2} & A_2\tanh(BR) \end{pmatrix} \tag{13}$$

Our diabatic basis chosen here is such that it does not explicitly depend on the nuclear coordinate R. The electronic Hamiltonian is written in matrix notation, with the matrix elements explicitly given by $H_{\mathrm{el}}^{jk}(R) = \int dq\phi_j^*(q)H_{\mathrm{el}}\phi_k(q) = \langle j|H_{\mathrm{el}}|k\rangle$.

We consider two cases (all numbers in atomic units): (a) $A_2 = -0.01$ and (b) $A_2 = 0.005$, with common parameters $A_1 = 0.01$, $B = 0.6$, $C = 0.001$, and $D = 1$. The potential, particularly in case (a), is motivated by Tully model 1 of ref 1.

The adiabatic potential energy surfaces obtained by solving $H_{\mathrm{el}}\phi_j^{\mathrm{ad}}(R) = E_j(R)\phi_j^{\mathrm{ad}}(R)$ for cases (a) and (b) can be seen in Figure 1. Case (a) is designed for an avoided crossing where the adiabatic surfaces are not parallel, while for case (b), these surfaces are nearly parallel.

The dynamics of these model systems can be solved numerically exactly. Details of this numerically exact dynamics is provided in the Appendix, and an open-source Python code for the exact quantum dynamics for the above systems is provided in ref 19. In brief, we first calculate the eigenfunctions and eigenenergies of the total Hamiltonian of eq 13: $H\Psi_k = E_k\Psi_k$. The time-dependent wave function can then be written as $\psi(t) = \sum_k c_k\Psi_k e^{-iE_k t/\hbar}$, where $c_k = \langle\Psi_k|\psi(0)\rangle$. For these simulations, we have chosen

https://doi.org/10.1021/acsomega.2c04843
ACS Omega 2022, 7, 45810−45824

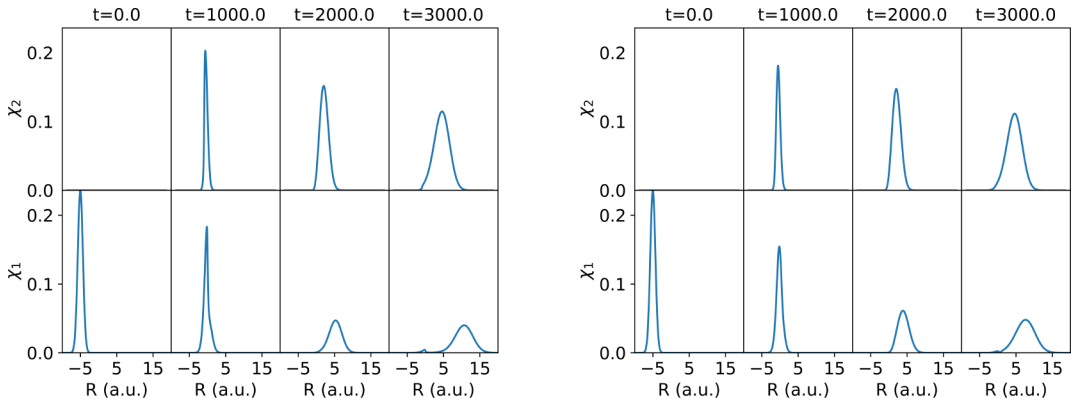

Figure 2. Absolute values of the nuclear wave functions, calculated numerically exactly, at different time steps (in au) along the evolution for cases (a) nonparallel and (b) nearly parallel potential energy surfaces. The lower and upper panels show the component of the wave packets on the ground adiabatic surface and excited adiabatic surface, respectively. Note the greater separation of wave packets for case (a) when surfaces are not parallel compared to case (b) where surfaces are nearly parallel.

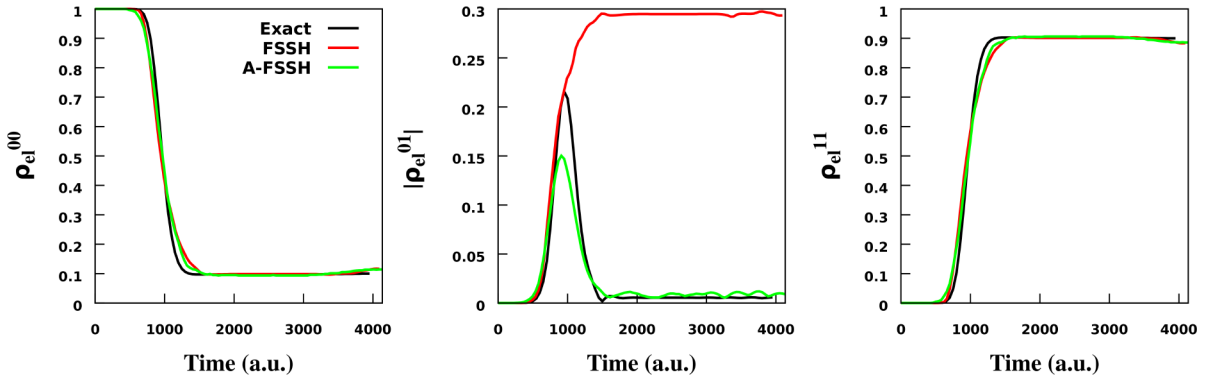

Figure 3. Absolute values of the electronic density matrix for nonparallel surfaces (corresponding to Figure 1(a)) as a function of time computed numerically exactly and using FSSH (without decoherence) and A-FSSH (with decoherence). Python codes are available for exact quantum dynamics in ref 19 and FSSH in ref 18.

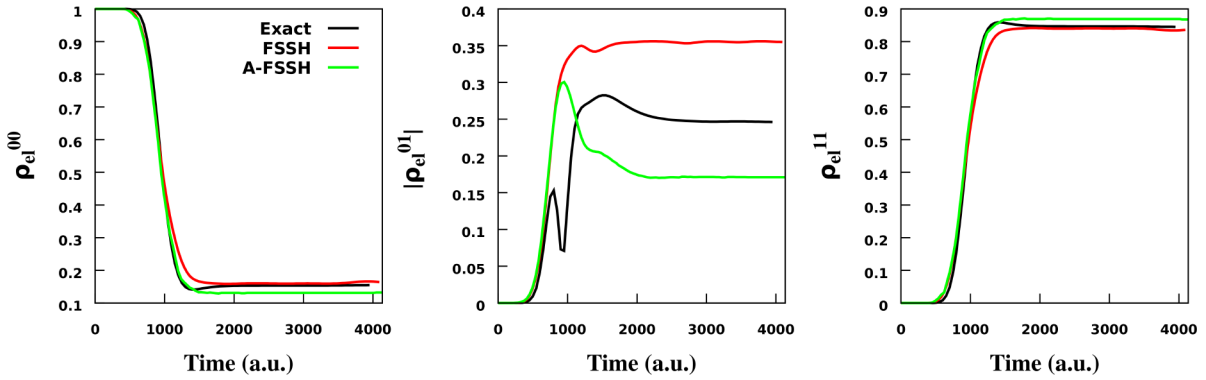

Figure 4. Same as in Figure 3 but for nearly parallel energy surfaces of Figure 1(b).

$\psi(R, 0) = N \exp\left(-\frac{(R-R_0)^2}{\sigma^2}\right) e^{ikR}|1\rangle$ with $R_0 = -5$ au, $\sigma = 1$ au, and $k = 11$ au. $|1\rangle$is the left diabat.

We expand the total wave function using eq 4 as

$$|\psi(R, t)\rangle = \chi_1(R, t)|\phi_1^{ad}(R)\rangle + \chi_2(R, t)|\phi_2^{ad}(R)\rangle \quad (14)$$

The numerically exact dynamics of $\chi_1(R)$ and $\chi_2(R)$ was computed using the procedure described in the Appendix. Absolute values of $\chi_1(R)$ and $\chi_2(R)$ can be seen in Figure 2. Once the wave function crosses the nonadiabatic coupling region, it "spawns" a new wave function on the upper adiabat, which then follows its dynamics. If the surfaces are not parallel, then the centers of the wave packets separate as time progresses, as can be seen in case (a) in Figure 2a. For case (b), however, since energy surfaces are nearly parallel, the wave packet separation is smaller on the time scale shown in Figure 2b.

To understand the relevance of decoherence, we calculate the electronic density matrix given by eq 5 in the adiabatic basis using numerically exact dynamics[19] as well as with FSSH simulations. For FSSH, we have calculated the adiabatic density matrix as $\rho_{el}(i, j) = c_i{}^* c_j$, averaged over 100 trajectories.

https://doi.org/10.1021/acsomega.2c04843
ACS Omega 2022, 7, 45810−45824

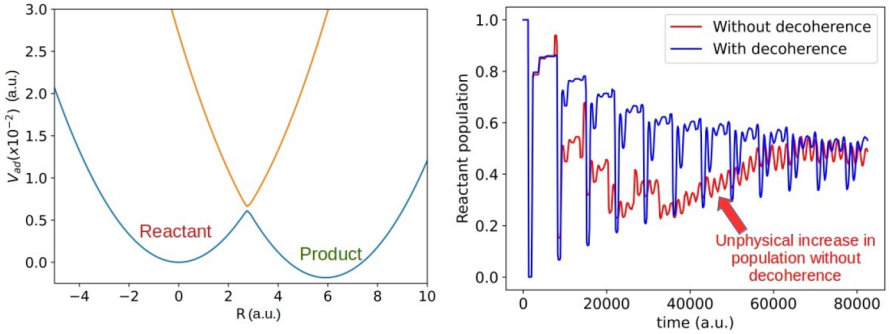

Figure 5. Reproduced from ref 22. Copyright [2015] American Chemical Society. (a) Plot of the adiabatic potential energy surfaces for the Hamiltonian of eq 17. (b) Reactant population decay averaged over 2000 trajectories calculated with and without decoherence. Decoherence is included from the augmented-FSSH version.[24,25]

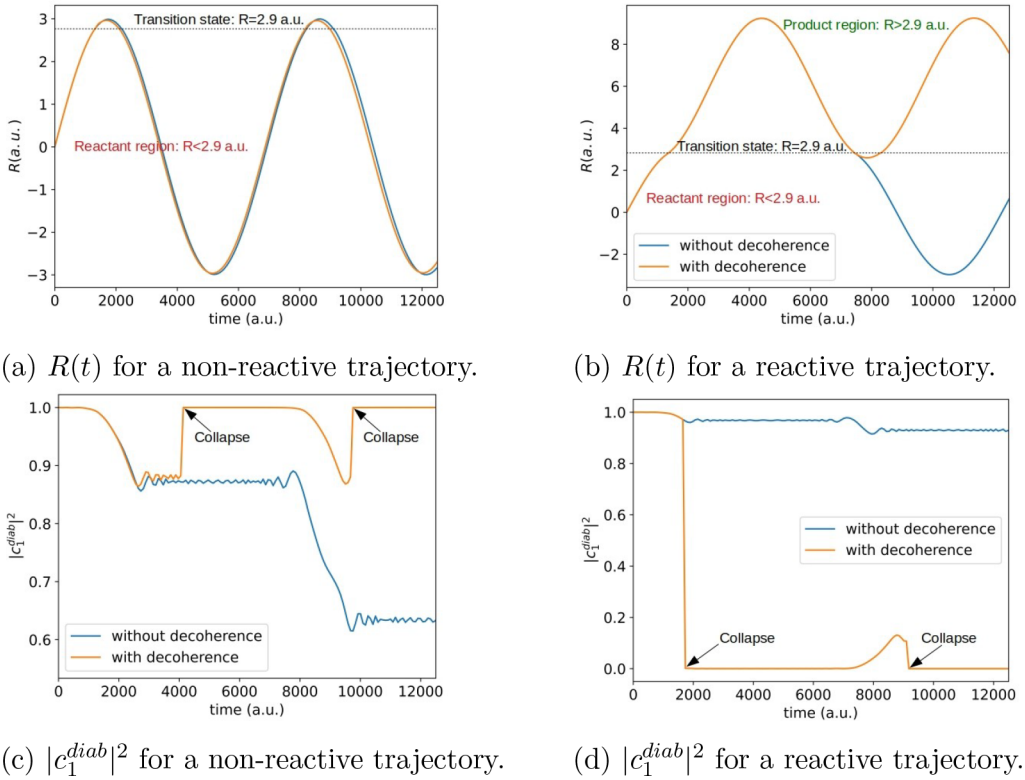

(a) $R(t)$ for a non-reactive trajectory.

(b) $R(t)$ for a reactive trajectory.

(c) $|c_1^{diab}|^2$ for a non-reactive trajectory.

(d) $|c_1^{diab}|^2$ for a reactive trajectory.

Figure 6. Reproduced from ref 22. Copyright [2015] American Chemical Society. Plot of position vs time for (a) a nonreactive and (b) a reactive trajectory. Corresponding plots of $|c_1^{diab}|^2$ are shown in (c) for the nonreactive trajectory and (d) for the reactive trajectory. The calculations are performed with the FSSH method with and without decoherence.

A Python code for FSSH is available in ref 18. Details of numerically exact dynamics are provided in Appendix.

Figures 3 and 4 show the electronic density matrix's diagonal and off-diagonal (absolute value) elements for the two cases. First, let us consider the numerically exact results. The diagonal elements behave roughly the same for the two cases. However, the off-diagonal element decays to 0 for Figure 3 (nonparallel surfaces), while it remains nonzero for Figure 4 (nearly parallel surfaces).

FSSH captures the diagonal element of the density matrix very well for both cases (Figures 3 and 4). However, the off-diagonal element remains large for both cases from the FSSH simulation. FSSH by itself does not capture the decay of the off-diagonal density matrix elements.

Decoherence is the decay of the off-diagonal elements of the density matrix. The inability of FSSH to capture this decoherence is the overcoherence issue of FSSH.

Let us briefly examine the origin of decoherence. Calculating the coherence term by substituting eq 4 in eq 5 gives

$$\langle \phi_k(R)|\rho_{el}(t)|\phi_{k'}(R)\rangle_q = \mathrm{Tr}_R(\chi_k(R,t)\chi_{k'}^*(R,t)) \quad (15)$$

$$= \langle \chi_{k'}(t)|\chi_k(t)\rangle_R \quad (16)$$

where $\langle \cdots \rangle_q$ is an integral over q variables and $\langle \cdots \rangle_R$ is an integral over R variables. Therefore, the coherences of the electronic density matrix decay as the overlap of the "nuclear" wave functions decays.

From a semiclassical perspective, the separation of the wave packets happens when the trajectories on different electronic

https://doi.org/10.1021/acsomega.2c04843
ACS Omega 2022, 7, 45810−45824

surfaces separate. This separation can occur due to either different forces or different momenta on the various electronic surfaces. When surfaces are parallel, coherence decay is due to differences in momenta, while when surfaces are not parallel, the coherence decay is due to differences in forces and momenta.

For the case of nearly parallel surfaces shown above, decoherence is not observed because our initial conditions are such that the momenta on the different surfaces are not significantly different. For cases with significant momenta differences, even on parallel energy surfaces, the wave packets will separate on different surfaces, and decoherence will occur.

4.2. Consequences of Not Including Decoherence. If surface hopping is used to examine ultrafast excited-state decay through avoided crossings or conical intersections, decoherence might not be necessary. If all that one cares about are the diagonal elements of the density matrix and the nonadiabatic event occurs only once during the course of dynamics, decoherence might not play an important role.

The story is entirely different if one is interested in long-time thermal populations or where the nonadiabatic region is encountered multiple times. To illustrate, consider a harmonic Hamiltonian (taken from ref 22):

$$H = \frac{p^2}{2m} + \begin{pmatrix} 1/2m\omega^2 R^2 & V_c \\ V_c & 1/2m\omega^2(R - R_0)^2 + \epsilon_0 \end{pmatrix} \quad (17)$$

As an example, for the parameters $V_c = 2.28 \times 10^{-4}$ au, $\omega = 9.1 \times 10^{-4}$ au, $R_0 = 5.91$ au, and $\epsilon_0 = 1.82 \times 10^{-3}$ au, FSSH simulations were run with fixed initial conditions: $R = 0$ au and initial energy $E_0 = 7.29 \times 10^{-3}$ au with positive momentum.[22] Decoherence is included within the augmented-FSSH method.[23] Open-source codes can be found in ref 24. Figure 5(a) shows the potential energy surfaces.

The reactant population was calculated as the fraction of trajectories with $R < 2.9$ au and active state $\lambda = 1$. Figure 5(b) shows the plot of population decay as a function of time with and without decoherence averaged over 2000 trajectories. The sharp lines in the population decay are due to constant energy calculations with fixed initial conditions. Two important things to note for population decay without decoherence: (1) the reactant population computed without decoherence initially (around t = 10 000 au) decays faster than the reactant population computed with decoherence and (2) after $t >$ 40 000 au, there is a nonphysical increase in the reactant population for calculations without decoherence.

To understand these nonexponential dynamics, consider the trajectories approaching the avoided crossing (transition state) from the left (reactant) region. We consider two kinds of trajectories: nonreactive and reactive. Nonreactive trajectories hop at the transition state, reflect on the excited state, and hop back to the ground state on reaching the transition state. These then proceed back to the reactant region. Reactive trajectories are the ones that do not hop and evolve to the right (product) region. To analyze these trajectories, we expand the electronic wave function in the diabatic basis: $\psi_{el} = c_1^{diab}|1\rangle + c_2^{diab}|2\rangle$.

Figure 6(a) and (c) shows the plots of R and $|c_1^{diab}|^2$ as a function of time for a nonreactive trajectory with and without decoherence. Since the trajectory is nonreactive, the position plot is nearly identical—the trajectories on reaching close to the transition state hop to the excited state and thereafter return to the reactant region. However, the plot of $|c_1^{diab}|^2$ is different with and without decoherence. $|c_1^{diab}|^2$ changes from 1 to about 0.85 after the first crossing of the transition state ($t \approx$ 2000 au). When the trajectory returns back to the reactant region, without decoherence $|c_1^{diab}|^2$ remains unchanged and on second crossing (at $t \approx$ 9000 au) changes to about 0.6. The change in $|c_1^{diab}|^2$ is 0.25 (= 0.85−0.6) after the second crossing, which is larger than the change in $|c_1^{diab}|^2$ of 0.15 (= 1−0.85) after the first crossing without decoherence. With decoherence, on returning to the reactant region, there is a collapse to the ground state (at $t \approx$ 4000 au), and on reaching the second crossing, $|c_1^{diab}|^2$ changes again from 1 to 0.88.

The larger change in quantum probabilities without decoherence is the reason the reactant population initially decayed faster without decoherence in Figure 5(b).

Now we examine a reactive trajectory, with and without decoherence, as shown in Figure 6(b) and (d). This trajectory does not hop on the first recrossing (at $t \approx$ 2000 au) and evolves to the product region. The potential energy surface dictating the dynamics in this region is the diabat $|2\rangle$. Without decoherence, however, $|c_1|^2 \approx 1$; i.e., the quantum amplitudes have not adjusted to the change in diabat. Including decoherence correctly resets the amplitude $c_1^{diab} \approx 0$ (and $c_2^{diab} \approx 1$) and sorts this problem. (Decoherence happened on the adiabatic surface, i.e., $c_1^{ad} = 1$ and $c_2^{ad} = 0$. However, since far away from the crossing diabat 2 is approximately the same as adiabat 1, $c_1^{ad} \approx c_2^{diab}$.) When this trajectory returns to the transition state from the product region, without decoherence, the quantum amplitudes behave as if the trajectory is returning on diabat 1 (i.e., with $c_1^{diab} = 1$), giving rise to a spuriously large probability of returning to the reactant region.[22]

Reference 22 provides a more detailed discussion on this. The incorrect high probability of a trajectory to go from product region to reactant region without decoherence results in the nonphysical increase in the reactant population without decoherence in Figure 5(b).

The nonexponential dynamics and incorrect time scale of decay without decoherence remain even when a thermal bath is included. If a thermal bath is added to the Hamiltonian of eq 17 to simulate the condensed phase, under certain regimes, exact quantum dynamics can be done (using the hierarchical equation of motion[26−29] in a strong system bath coupling regime), and Marcus theory can be used under certain regimes (weak diabatic coupling).

When the results of FSSH without any decoherence are benchmarked against those of numerically exact results and Marcus theory, the rate constants are too fast compared to the correct results. Including decoherence corrects this issue in large part.[22,23,30]

4.3. Methods to Include Decoherence. Different decoherence algorithms exist that set criteria based on which, after coherences are created, typically in the adiabatic basis, the quantum amplitudes are reset.

The simplest and cheapest decoherence scheme is to set a threshold value for the adiabatic energy difference. Once a trajectory has an adiabatic energy difference less than this threshold, the trajectory has entered a region with strong nonadiabatic coupling. After the trajectory exits this region (based on the energy threshold criteria), the amplitudes are reset to 1 for the active state and 0 for the rest.[31,32]

The above scheme is clearly too simple to be applicable to all cases. For a generalized decoherence method, the works of Bittner, Prezhdo, Shwartz, Truhlar, and Rossky showed that within the frozen Gaussian approximation[33] the decoherence

https://doi.org/10.1021/acsomega.2c04843
ACS Omega 2022, 7, 45810−45824

rate is proportional to the force difference between the adiabatic states.[34−39] The main difference between the different approaches is estimating the proportionality constant. Another approach was to estimate the decoherence time scale as proportional to the adiabatic energy difference, proposed originally by Zhu and Truhlar[40,41] and later implemented by Granucci et al.[42] An alternate was further proposed by Jasper and Truhlar that accounts for both the differences in momenta and the differences in forces of the potential energy surfaces.[43] Later, the Subotnik group derived a decoherence rate (within the frozen Gaussian approximation)[23,25] by mapping the FSSH method within certain approximations to the quantum-classical Liouville equation.[44] This scheme requires the evolution of extra variables to estimate the time scale of separation of wave packets on different surfaces.

The decoherence version of choice depends on the problem under study. If there is one sharp avoided crossing, the most straightforward choice of collapsing based on a threshold adiabatic energy difference might work (though one should ensure that the results are independent of the cutoff parameter chosen). For more general cases, different decoherence schemes can be chosen depending on the complexity of the problem and the resources available.

5. ELECTRONIC DENSITY MATRIX

One is often interested in the population of a given diabatic or adiabatic state. If the diabatic coupling is weak, the simplest approach is to calculate the adiabatic populations as the fraction of trajectories on that adiabat. In the limit of weak diabatic coupling, diabatic populations can be mapped to adiabatic populations. *Using quantum amplitudes often gives spurious results—the quantum amplitudes at long times are unreliable.* FSSH often does not follow internal consistency; i.e., the fraction of trajectories on a given adiabat i is not equal to $|c_i^2|$. This point is discussed further in Section 6.

When the diabatic coupling is large and extended over a large coordinate space, a simple mapping between the diabatic and the adiabatic populations might not be possible. For such cases, the diabatic population cannot be calculated simply using the fraction of trajectories on adiabatic surfaces.

A different approach was developed by the Subotnik group, where they connected the surface hopping approach with the quantum-classical Liouville equation (under certain approximations).[44,45] Motivated by the quantum-classical Liouville equation, a better choice for the adiabatic electronic density matrix was shown to be[46]

$$\rho_{\mathrm{el}}^{\mathrm{ad}}(i,j) = \begin{cases} \delta_{i\lambda} & i = j \\ c_i^* c_j & i \neq j \end{cases} \tag{18}$$

where λ is the active state.

Once the adiabatic density matrix is known, it can be easily transformed to any other diabatic basis of choice and averaged over an ensemble of trajectories.

Let us illustrate the above approach using an example: for a two-level electronic system, we define the Hamiltonian in the diabatic states $|1\rangle$ and $|2\rangle$:[47]

$$H = \begin{pmatrix} 0 & V_c \\ V_c & \epsilon_0 \end{pmatrix} + \sum_i \left(\frac{p_i^2}{2m} + \frac{1}{2} m\omega_i^2 q_i^2 \right) + \begin{pmatrix} \sum_i g_i q_i & 0 \\ 0 & -\sum_i g_i q_i \end{pmatrix} \tag{19}$$

Equation 19 describes the spin-Boson Hamiltonian and is often used to describe condensed-phase electron transfer.[47] The couplings g_i are described using spectral density function, chosen here to be Drude spectral density: $J(\omega) = \frac{\pi}{2}\sum_i \frac{g_i^2}{m\omega_i}\delta(\omega - \omega_i) = 2\lambda\frac{\gamma\omega}{\gamma^2+\omega^2}$. The dynamics of this particular Hamiltonian can be computed numerically exactly using a method called the hierarchy equation of motion (HEOM).[26−29]

For the choice of parameters $V_c = 87$ cm^{-1}, $\epsilon_0 = 120$ cm^{-1}, $\lambda = 70$ cm^{-1}, $\gamma = 20$ ps^{-1}, and $T = 77$ K,[48] we calculate the population of diabat $|1\rangle$ using FSSH and numerically exact computation (codes available in ref 49). Initially, the system starts with diabat $|1\rangle$ and the bath at thermal equilibrium. FSSH simulations are performed with the Drude spectral density first transformed to the Brownian spectral density for efficient simulations—details of this can be found in ref 49. 2000 FSSH trajectories are evolved with a time step of 0.2 fs. For FSSH, we have calculated the populations using eq 18 as well as using quantum coefficients in the diabatic basis: $P_1 = |c_1^{\mathrm{diab}}|^2$. Results are compared both with and without decoherence. Decoherence was included using the augmented FSSH approach.

Figure 7 shows the comparison of the diabatic populations calculated from different approaches. This system is particularly chosen where the diabatic coupling is large (87 cm^{-1}) such that the diabatic populations and the adiabatic populations will be very different. In this case, note that usage of eq 18 gets results closer to the numerically exact results (although not exactly the same). Populations calculated

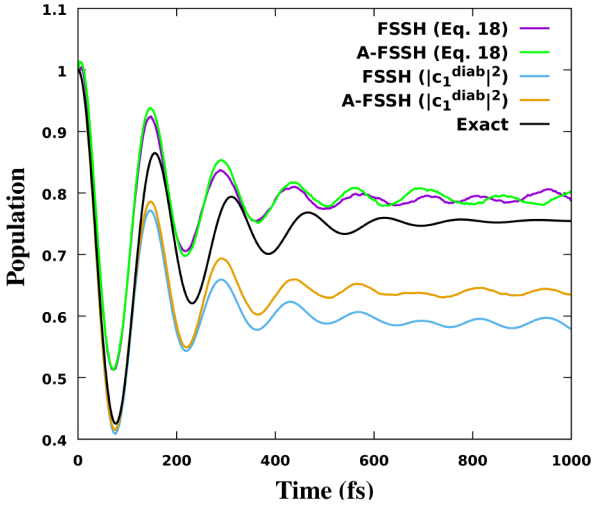

Figure 7. Population of diabat 1 as a function of time calculated using numerically exact simulations (HEOM), FSSH using diabatic coefficients, and eq 18. FSSH populations were calculated with and without decoherence. Decoherence was included using the augmented FSSH (A-FSSH) approach.

https://doi.org/10.1021/acsomega.2c04843
ACS Omega 2022, 7, 45810−45824

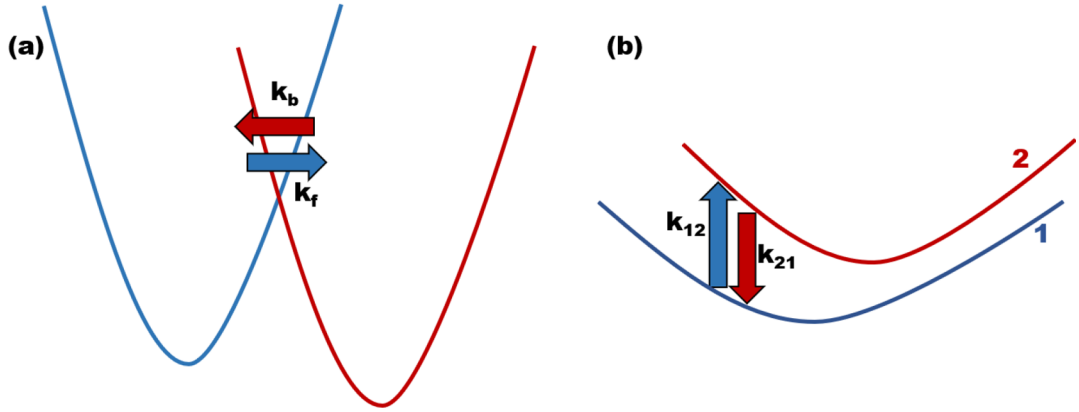

Figure 8. Schematic figure of potential energy surfaces for (a) forward and backward rate constants for a reaction and (b) transitions between energetically accessible energy surfaces.

using diabatic coefficients, with or without decoherence, are relatively worse. Another point worth noting is that all the methods get the early dynamics (t < 100 fs) correct.

The parameters above were specifically chosen to demonstrate that quantum coefficients might not always be reliable. For smaller diabatic couplings V_c, the results from the different approaches will agree.

6. FRUSTRATED HOPS

When a hop occurs, velocity is rescaled (typically along the direction of the nonadiabatic coupling vector $d_{\lambda k}$) to conserve energy. While hopping to an excited state, if enough energy does not exist to rescale the velocity, the hop is called frustrated. *Frustrated hops in FSSH are important to include since these frustrated hops give rise to detailed balance.*[50] See Section 7 for a discussion.

Different strategies exist to handle frustrated hops. The simplest option is not to hop and continue evolving on the original state. Another commonly used option is to reverse velocity along the $d_{\lambda k}$ direction.

Truhlar's group has systematically and exhaustively studied different options and proposed a simple scheme for a frustrated hop: reverse velocity only when the forces along the derivative coupling have opposite signs.[51−53] The central "intuition" behind this scheme is that if the forces have opposite sign, a hop to the excited state is likely to reverse velocity.

Velocity reversal is, in fact, crucial for condensed phase dynamics. FSSH recovers the Marcus rate constants only when this velocity reversal is included.[30] To understand this, consider the potential energy surface of Figure 5(a). It is easy to see that the energy difference between the two adiabats at the point of crossing is $2V_c$. Once more, consider trajectories approaching the avoided crossing from the left, which we call the reactant region. Let us say that the probability of not hopping at a given energy is $p(E)$. That is, the probability of a trajectory being reactive at energy E is $p(E)$. At thermal equilibrium, the net probability of the reaction per crossing event is

$$p(T) = \int_{V_b}^{\infty} \mathrm{d}E p(E) \tag{20}$$

where V_b is the barrier height. If this is averaged with the frequency of reaching the crossing point, one gets the total rate constant. In the limit of small V_c, Fermi's golden rule (or its classical limit, Marcus theory) gives $p(E) \propto V_c^2$. This gives an overall rate constant proportional to V_c^2.

So far, we have not included frustrated hops in the description. All trajectories with an energy between V_b and $V_b + 2V_c$ will experience a frustrated hop. *If velocity is never reversed on a frustrated hop, $p(E) = 1$ for such trajectories.* We, therefore, modify our net probability as

$$p(T) = \int_{V_b}^{V_b+2V_c} dE p(E) + \int_{V_b+2V_c}^{\infty} \mathrm{d}E p(E) \tag{21}$$

$$= 2V_c + \int_{V_b+2V_c}^{\infty} \mathrm{d}E p(E) \tag{22}$$

The effect of never reversing velocity on a frustrated hop is that the rate becomes proportional to V_c in the limit of small V_c, which is inconsistent with the correct Fermi's golden rule (or Marcus) result.[54]

Before closing this section, we make one additional remark regarding internal consistency in FSSH. One immediate consequence of frustrated hops is that they lead to inconsistency between $|c_i^2|$ and fraction of trajectories on an adiabatic surface i.[9,21,55] This inconsistency can exist even without frustrated hops due to divergent trajectories.[20] Therefore, to calculate the population of a given adiabatic surface, using $|c_i^2|$ might lead to erroneous results as was discussed in Section 5. We also note that adding decoherence can partially improve the internal consistency in FSSH.[21,56]

7. TIME REVERSIBILITY AND DETAILED BALANCE

FSSH does not obey time reversibility.[57,58] Within classical mechanics, imagine simulating a system with some initial conditions for some duration t. At this time, t, we reverse all the velocities ($v = -v$) and evolve the system again for the same duration t. Assuming the forces are independent of time, the system will retrace its steps back to the initial conditions.[59,60] Now let us imagine doing the same with FSSH. Some of the trajectories might hop during the time interval t. Because FSSH is stochastic (i.e., hops are determined using a random number), after reversing the velocities, these trajectories might not hop at the same time step as when they hopped in the forward evolution. Therefore, not all trajectories will return to the initial conditions for FSSH.

It can be shown that if time reversibility holds then detailed balance also holds.[60] Detailed balance refers to a system

https://doi.org/10.1021/acsomega.2c04843
ACS Omega 2022, 7, 45810−45824

attaining correct thermal equilibrium at long times. This raises the question as to whether FSSH obeys detailed balance.[50,61−63]

There are two related questions we consider: (a) for a reaction at a constant temperature with a barrier, will FSSH give detailed balance for the thermal rate constants, and (b) will the ratio of the populations of different adiabatic surfaces calculated from FSSH obey detailed balance?

Let us start with the first question: why should the thermal rate constants calculated from FSSH obey detailed balance? Figure 8(a) shows a schematic of a potential energy surface. The forward thermal rate constant (i.e., from reactant to product) can be evaluated as $k_f(T) = \int_0^\infty dE \kappa_f(E) g_R(E) e^{-\beta(E-E_r)}$, where E_r is the reactant minimum energy; $g_R(E)$ is the degeneracy of reactant states with energy E; and $\kappa_f(E)$ is the microcanonical forward rate constant, that is, the forward rate constant at a constant energy E. Similarly, the backward thermal rate constant (i.e., from product to reactant) can be evaluated as $k_b(T) = \int_0^\infty dE \kappa_b(E) g_P(E) e^{-\beta(E-E_P)}$, with E_p being the product minimum energy, $g_P(E)$ being the degeneracy of product states at energy E, and $\kappa_b(E)$ being the backward microcanonical rate constant. If time reversibility holds, then it can be shown that $\kappa_f(E) g_R(E) = \kappa_b(E) g_P(E)$.[59,60]

An investigation by the Subotnik group shows that for a case with $g_R(E) = g_P(E)$, although FSSH gives different forward and backward microcanonical rate constants (i.e., $\kappa_f(E) \neq \kappa_b(E)$) when averaged over energy E, FSSH does get the forward and the backward rate constants approximately equal ($\langle \kappa_f(E) \rangle \approx \langle \kappa_b(E) \rangle$).[54] This averaging is the savior of FSSH: a thermal average of the microcanonical rate constants gives a thermal rate constant, which approximately obeys the detailed balance in FSSH.

It is important to note that the above discussion holds only when decoherence is included, as discussed in Section 4. *Without decoherence, the population decay might not be exponential at all (that is, FSSH might give erroneous kinetics, and the rate constants might not be well-defined).*[22] Further decoherence has been shown to improve detailed balance in FSSH.[64]

Second, consider the schematic shown in Figure 8(b), with two electronic surfaces labeled 1 and 2, with $E_{12} = E_2 - E_1 > 0$. Assuming classical velocities are at thermal equilibrium, the ratio of the FSSH hopping rates between these surfaces is[5,61]

$$\frac{k_{1\to 2}}{k_{2\to 1}} = \frac{\int_{-\infty}^{\infty} dv e^{-1/2\beta m v^2} |T_{21}| Re(c_1^{1*} c_2^1) |p_{allow}^{1\to 2}(v)}{\int_{-\infty}^{\infty} dv e^{-1/2\beta m v^2} |T_{12}| Re(c_1^{2*} c_2^2) |p_{allow}^{2\to 1}(v)} \quad (23)$$

where v is the classical velocity; $\beta = 1/k_B T$ is the inverse temperature; $p_{allow}^{i\to j}(v)$ is the probability that the hop is not frustrated; and c_i^j is the quantum amplitude c_i evolving on surface j.

Here we make another important assumption: c_i^j is independent of surface j as well as the velocity v. Noting $|T_{12}| = |T_{21}| = |v d_{12}|$, $p_{allow}^{2\to 1}(v) = 1$, and $p_{allow}^{1\to 2}(v) = h(v_0)$, where h is the Heaviside function and $1/2 m v_0^2 = E_{12}$, we get

$$\frac{k_{1\to 2}}{k_{2\to 1}} = \frac{2\int_{v_0}^{\infty} dv e^{-1/2\beta m v^2} v}{2\int_0^{\infty} dv e^{-1/2\beta m v^2} v} \quad (24)$$

Using substitution of variables $E = 1/2\ mv^2$, it is now easy to show that

$$\frac{k_{1\to 2}}{k_{2\to 1}} = e^{-\beta E_{12}} \quad (25)$$

In deriving this, we have assumed (a) the velocity to be at thermal equilibrium and (b) the quantum coefficients to be independent of the velocity as well as independent of the surface of evolution. These approximations are not exactly met, and therefore FSSH does not give an exact detailed balance; however, usually, the thermal populations from FSSH are close to the correct Boltzmann answer.

Finally, we note that the Boltzmann condition in eq 25 is derived, assuming that the hopping probability is proportional to the velocity (via the T_{12} term). This is true in the adiabatic basis; however, if FSSH is being done in a diabatic basis, this might not be true, and one should be careful.

8. VIBRATIONAL QUANTIZATION

We in this section discuss a case study where all the details of the FSSH simulation are important to treat correctly to get the correct rate constants.

Although surface hopping simulations generally are used for electronic nonadiabaticity, they can treat vibrational quantum effects on the same footing. The separation of q and R is on the user, and the vibrational modes can be included in the quantum q modes. Hammes-Schiffer's group has arguably studied this extensively in the context of proton and hydrogen transfer.[31,32,65−68]

Vibrational quantization within FSSH is ideal when nuclear quantum effects of only 1 or 2 modes are important, for example, proton transfer (or related reactions), where quantum nuclear effects of only the transferring H atom are important. Including more vibrational modes quantum mechanically becomes too computationally expensive.

Vibrationally quantized surface hopping has long been used for electronically adiabatic problems (i.e., dynamics is confined to a single electronic potential energy surface). Benchmarking for this has been done to show that surface hopping works well for a broad range of parameters.[69,70] Recent benchmarking of the surface hopping method has also been done to capture quantum nuclear effects for electronically nonadiabatic problems.[49]

Simultaneous vibrational and electronic nonadiabaticity is one of the extreme cases for FSSH, where all the nuances must be treated correctly to get the correct rate constants. Including decoherence is challenging since both parallel and nonparallel surfaces are present. The decoherence scheme chosen should include contributions to the decoherence rates from both parallel and nonparallel surfaces. Similarly, if velocity is never reversed on a frustrated hop, the decay rate constants can be much faster (see results below for a specific example). Further, this is a case where the diabatic couplings (between vibronic levels) can be small. Therefore, the method should be able to deal with trivial crossings correctly and efficiently (see Section 9 for a discussion).

From a surface hopping perspective, quantum nuclear effects emerge as vibrational nonadiabaticity, i.e., avoided crossings in vibronic potential energy surfaces. As a concrete example,[49] let us modify the Hamiltonian of eq 17 to

$$H = \frac{p_x^2}{2m} + H_{qm} \quad (26)$$

https://doi.org/10.1021/acsomega.2c04843
ACS Omega 2022, 7, 45810−45824

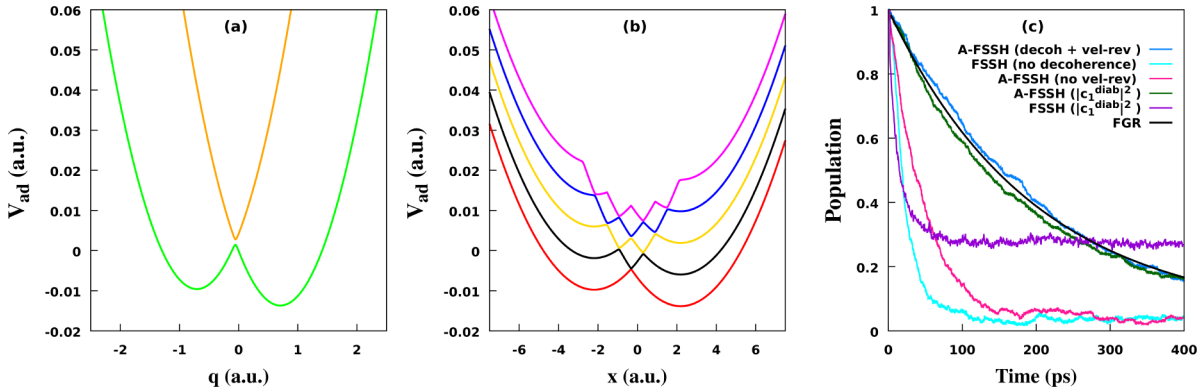

Figure 9. Reproduced from ref 49. Copyright [2021] American Chemical Society. (a) The electronic adiabatic potential energy curves of eq 27 as a function of q (keeping x at equilibrium: $x = gq$), (b) the vibronic energy surfaces as a function of mode x treating q quantum mechanically, and (c) population decay as a function of time using FSSH simulations compared to the Fermi's golden rule population decay.

$$H_{qm} = \frac{p_q^2}{2m} + \begin{pmatrix} 1/2m\omega_1^2 q^2 & V_c \\ V_c & 1/2m\omega_1^2(q - q_0)^2 + \epsilon_0 \end{pmatrix} + \frac{1}{2}m\omega_2^2(x - gq)^2 \tag{27}$$

To treat q quantum mechanically, the vibronic adiabatic energies are calculated by solving

$$H_{qm}\psi_i^{ad}(q, x) = E_i^{ad}(x)\psi_i^{ad}(q, x) \tag{28}$$

The energy surfaces $E_i^{ad}(x)$ are called vibronic potential energy surfaces.

For the choice of parameters $m = 1$ amu, $V_c = 6.8 \times 10^{-4}$ au, $\omega_1 = 0.0054$ au, $\omega_2 = 0.0018$ au, $\epsilon_0 = 0.0041$, $q_0 = 1.4$ au, and $g = 0.0058$ au (taken from ref 49), the potential energy surfaces along the q coordinate are shown in Figure 9(a) (with $x = gq$). If frequency ω_1 of the q mode is large ($k_BT \ll \hbar\omega_1$), then quantum effects such as tunneling for q mode cannot be ignored. After quantization of q, x becomes the reaction coordinate, and the potential energy surfaces are shown in Figure 9(b). Now we note that the barrier height is much smaller along the x direction, but one gets many more crossings with much smaller energy gaps. That is, the quantum nuclear effects show up as vibrational nonadiabaticity. We also note that after quantization some of the vibronic surfaces are nearly parallel, while some are not.

To calculate thermal rates, FSSH simulations are performed for the above Hamiltonian with a Langevin friction (with friction constant $\gamma = \omega_2$ and $k_BT = 0.0013$ au) added to the x mode. We compute results from FSSH with decoherence added (A-FSSH version), velocity reversed on a frustrated hops (Truhlar's scheme), and using eq 18 to compute diabatic populations. Codes for these calculations can be found at ref 71. These population decay results are compared against those computed when there is (a) no decoherence (see Section 4), (b) velocity is not reversed on a frustrated hop (see Section 6), or (c) population is computed using diabatic quantum coefficients alone: $P_i = |c_i^{diab}|^2$ (see Section 5).

Population decay from the different approaches is shown in Figure 9(c). These results are compared against Fermi's golden rule (FGR) result, which is exact for small diabatic coupling V_c. A good comparison with FGR results is obtained when all the nuances are correct. In the absence of decoherence or no velocity reversal on frustrated hops, the results are much faster. Using quantum coefficients to compute population gives correct results only with decoherence. In the absence of decoherence, $|c_i^{diab}|^2$ gives the wrong long-time population.

Although doing surface hopping simulations on vibronic surfaces (E_i^{ad}) is no different from electronic surface hopping, one has to pay extra attention to the details.

- Multiple vibronic levels must be used to converge results. Missing excited vibronic surfaces can lead to incorrectly large rate constants.
- The derivative coupling between the vibronic states can be large (owing to small Franck−Condon factors between vibrational wave functions). The surface hopping method used, therefore, must be robust to the presence of sharp avoided/trivial crossings. See Section 9 for a discussion.
- Small diabatic coupling is also the regime where velocity reversal on frustrated hops can play a crucial role. See Section 6 for a discussion. We recommend Truhlar's scheme for when to reverse velocities.[53]
- The vibronic surfaces present one of the most challenging cases for decoherence algorithms. Some of the surfaces are nearly parallel, while some are not. Therefore, the decoherence scheme used must include contributions to the decoherence rates from both parallel as well as nonparallel surfaces.

9. TRICKS OF THE TRADE

Here we provide some finer simulation details that become important for an efficient FSSH simulation, no matter the variant of FSSH being used.

9.1. Calculating Derivative Coupling. Evolution of a quantum subsystem as well as the calculation of hopping probabilities require the time-derivative coupling matrix $\mathbf{T}$ (with matrix elements $T_{jk} = \nu d_{jk} = \left\langle \phi_j^{ad}(R(t)) \middle| \frac{d}{dt}\phi_k^{ad}(R(t)) \right\rangle$). These can be calculated from an electronic structure calculation as

$$d_{jk} = \frac{\left\langle \phi_j^{ad}(R) \middle| \frac{\partial H_{el}}{\partial R} \middle| \phi_k^{ad}(R) \right\rangle_q}{E_k - E_j} \tag{29}$$

Derivation of this equation can be found in ref 31.

Using eq 29 is not efficient, though, and can even lead to missing some of the nonadiabatic couplings. Instead, modern packages calculate an averaged time derivative coupling[25,31,72]

https://doi.org/10.1021/acsomega.2c04843
ACS Omega 2022, 7, 45810−45824

$$\bar{\mathbf{T}} = \frac{1}{dt_c}\int_{t_0}^{t_0+dt_c} dt\,\mathbf{T}(\mathbf{t}) \tag{30}$$

$$= \frac{1}{dt_c}\log(\mathbf{U}(dt_c)) \tag{31}$$

where dt_c is the classical time step and $U_{jk}(dt_c) = \langle \phi_j^{ad}(R(t_0))\,|\phi_k^{ad}(R(t_0 + dt_c))\rangle$ is the overlap matrix. Derivation of eq 31 can be seen in ref 25.

The advantage of using eq 31 is 2-fold. First, instead of calculating the more expensive vector d_{jk}, one only calculates the scalar matrix $\mathbf{T}$. Second, suppose there is an avoided crossing or a trivial crossing (with diabatic coupling zero), then the derivative coupling vector will be very sharply peaked. In this case, if the classical position does not exactly land on these regions of strong derivative coupling, one can completely miss these sharp avoided/trivial crossings. With a time-averaged derivative coupling, however, one does not miss these strong derivative coupling regions.

9.2. Sign Choice of the Adiabatic Wave Function. In general, the sign of the adiabatic wave functions ϕ_j^{ad} is not uniquely defined. It is important, however, to fix a sign convention to avoid spurious results.[25]

The simplest choice is to choose any sign for each adiabatic wave function at the start of the simulation and use $\langle \phi_j^{ad}(R(t_0))|\phi_j^{ad}(R(t_0 + dt_c))\rangle > 0$ for later time steps.

Suppose this sign convention is not chosen. In that case, $U_{jj} \approx -1$ can hold in regions with negligible derivative coupling. One then gets complex derivative coupling (from eq 31). Even if eq 29 is used to calculate the derivative coupling vector, very small quantum time steps will be necessary for evolving c_j values.

At a trivial crossing, choosing the sign convention can be tricky, and we refer the reader to ref 25 for more details.

9.3. Separation of Time Steps. Classical and quantum subsystems typically have very different frequencies or time scales. Therefore, evolving these two subsystems with different time steps makes sense.[25,31]

One usually evolves the classical subsystem with a larger classical time step first. Time derivative coupling can then be calculated using eq 31, and quantum amplitudes evolved over a smaller quantum time step. The adiabatic energies can be linearly interpolated from t_0 to $t_0 + dt_c$ for this purpose.

The time step of the quantum subsystem is often about a factor of 10 smaller than the classical subsystem. For very sharp crossings, this can be even smaller. Some algorithms can automatically choose the quantum time step based on the strength of time derivative coupling and adiabatic energy differences.[25]

9.4. How to Collapse. One nuance about collapsing quantum amplitudes: when there are multiple energy surfaces present (more than 2), there can be different strategies to collapse the quantum amplitudes. One option is to reset the quantum amplitude to 1 for the active surface and 0 for the rest. However, most decoherence approaches calculate the decay rate of the off-diagonal element of the density matrix ρ_{ij}. From the FSSH perspective, one method to account for possibly different decay rates for different off-diagonal density matrix elements is to calculate the different collapse (decoherence) rates between the active state λ and all other states $j \neq \lambda$ at each classical time step. Now, based on a random number, if decoherence between the active state λ and a particular state j occurs, then the quantum amplitudes can be adjusted as[23]

$$c_\lambda^{new} = c_\lambda \frac{\sqrt{|c_\lambda^2| + |c_j^2|}}{|c_\lambda|} \tag{32}$$

$$c_j^{new} = 0 \tag{33}$$

$$c_k^{new} = c_k \quad k \neq j, \lambda \tag{34}$$

This approach resets the quantum amplitudes only for the state λ and one other state j at a time.

9.5. Overall Algorithm. A basic algorithm of FSSH, therefore, goes as

1. Create a loop over trajectories. Since trajectories are independent, each trajectory can be run over a different node.
   (a) For each trajectory, choose the initial position R, momentum P, active state λ, and quantum coefficients c_i. This choice depends on the problem being investigated.
   (b) Create a loop over time.
      i. At the current time step t_0, solve for eq 3 to get eigenfunctions $\phi_i^{ad}(R(t_0))$ and eigenenergies $E_i^{ad}(R(t_0))$.
      ii. Except for the first time step, if $\langle \phi_j^{ad}(R(t_0 - dt_c))|\phi_j^{ad}(R(t_0))\rangle < 0$, set $\phi_j^{ad}(R(t_0)) = -\phi_j^{ad}(R(t_0))$.
      iii. Calculate force as $F = -\nabla\langle \phi_\lambda^{ad}(R(t_0))|H_{el}|\phi_\lambda^{ad}(R(t_0))\rangle$.
      iv. Evolve R and P classically using a classical time step. Typically, the velocity−Verlet or Runge−Kutta fourth-order methods are good enough integrators.
      v. Use eq 31 to calculate time derivative coupling.
      vi. Evolve c_i's using eq 10 over a smaller quantum time step. Runge−Kutta fourth order is a common choice for the integrator.
      vii. While evolving c_i's, calculate the hopping probability using eq 12 over each quantum time step to each state k. Call a uniform random number r between 0 and 1. If $\sum_{l=1}^{k-1} g_{\lambda l} < r < \sum_{l=1}^{k} g_{\lambda l}$, store the label k until the classical time step is reached and do not check for any more hops.
      viii. At each classical time step, if a hop to state k was attempted during step 1(b)vii, calculate derivative coupling vector $d_{\lambda k}^n$ (where n refers to the nth classical coordinate). The velocity now needs to be rescaled as $v_n' = v_n - \gamma d_{\lambda k}^n/m_n$.[31] γ is calculated to conserve total energy. For that, calculate $a = \sum_n d_{\lambda k}^{n2}/(2m_n)$, $b = \sum_n v_n d_{\lambda k}^n$, and $c = E_k - E_\lambda$. Here m_n and v_n are the mass and velocity of the n'th coordinate, respectively. If $b^2 - 4ac > 0$, hop is not frustrated: set new state to k and calculate $\gamma = (-b \pm \sqrt{b^2 - 4ac})/(2a)$. The sign $\pm$ is chosen as the same as the sign of b. If $b^2 - 4ac < 0$, hop is frustrated,

https://doi.org/10.1021/acsomega.2c04843
ACS Omega 2022, 7, 45810−45824

and the state does not change. If velocity is to be reversed,[53] set $\gamma = b/a$.

ix. At each classical time step, check for decoherence based on the method of your choice. See Sec. 4 for discussion. Equations. 32-34 can be used to collapse c_i's.

x. Calculate any time-dependent observable if needed.

(c) Calculate any observable at the end of the simulation time if needed.

2. Average the observables over the trajectories.

A basic Python FSSH code following the above algorithm can be found in ref 18. A faster Fortran version, including decoherence, frustrated hops, and correct calculation of the density matrix, can be found in ref 24.

10. CHOICES FOR A PRACTITIONER

10.1. Should I Add Decoherence? *Yes.* There are situations where decoherence might not play a role, as discussed in examples in this overview. However, if one does not know a priori, and it is often unclear whether decoherence is important, it is better to add decoherence.

Importantly, adding decoherence will rarely worsen the surface hopping result (the only known exception is the additional broadening of spectra for gas-phase systems). Therefore, it is important to know if adding decoherence might have made a difference to the study.

Different packages for doing surface hopping simulations allow for different schemes available in the literature.[23,25,35,42]

10.2. What Method to Use for Frustrated Hops? This question might not even be relevant for photoexcited dynamics since the system has enough energy that no frustrated hops will be encountered. Nonetheless, Truhlar's scheme[53] of reversing velocity on encountering frustrated hop only when the adiabatic forces have opposite signs is a good one.

10.3. How to Average Diabatic Populations? If the adiabatic surfaces look close to the diabatic surfaces, the most straightforward strategy is to compute the fraction of trajectories on each adiabatic surface. For problems where this is not true, Subotnik's scheme is the preferred one.[46]

Using quantum amplitudes can give incorrect results as they are often unreliable at long times. That being said, quantum amplitudes often converge faster than the surface populations, and if it is known that they are accurate for the system under investigation, they can be used to reduce the number of trajectories.

11. CODES

Codes for performing numerically exact quantum dynamics with one coordinate R and two quantum states can be found at:

- Github link: https://github.com/amber-jain-group-iitb/Exact-QD-Python
- Static link: https://zenodo.org/badge/latestdoi/519436839

A detailed algorithm for the above codes is given in the Appendix. Codes for a basic implementation of the FSSH algorithm in Python are at:

- Github link: https://github.com/amber-jain-group-iitb/FSSH-Python
- Static link: https://zenodo.org/badge/latestdoi/519432030

The above FSSH codes follow the algorithm given in Section 9.5 and do not include decoherence or velocity reversal on frustrated hops.

The above libraries have commented codes and a detailed readme file with instructions for running the codes and how the codes are structured. We strongly encourage the reader to run the codes and modify the potentials (instructions in readme files) to compare exact vs FSSH dynamics. Readers with an elementary knowledge of Python coding are encouraged to add their decoherence scheme and velocity reversal on a frustrated hop in the provided FSSH codes.

A faster Fortran implementation of surface hopping with decoherence included using the augmented FSSH,[25] velocity reversal on frustrated hops treated based on Truhlar's scheme,[53] and correct calculation of diabatic populations[46] can be found at

- Github link: https://github.com/amber-jain-group-iitb/AFSSH
- Static link: https://zenodo.org/badge/latestdoi/189350184

12. CHALLENGES AND OPPORTUNITIES

The main criticism of surface hopping comes from the independent trajectory assumption. This is also why decoherence schemes are always approximate in surface hopping—true decoherence emerges from the correlation between different trajectories. Alternative methods exist to evolve trajectories in a coupled fashion.[33,73,74]

An extreme case of the coherence issue is the recoherence phenomenon. This recoherence occurs for gas-phase systems where two wave packets that have separated and come back together can interfere constructively or destructively. Such recoherences occur, for example, in the low friction regime of the spin-Boson model.[75] These recoherences also show up in the case of gas-phase spectroscopy.[76] Surface hopping cannot capture these recoherences.[77] However, a surface hopping approach based on the quantum-classical Liouville equation was shown to capture these recoherences for the spin-Boson model.[78]

Finally, on-the-fly surface hopping is mainly performed for low-dimensional systems due to high computational costs. There is a scope for developing tools for efficient on-the-fly methods with machine learning.[79]

13. CONCLUSION

Fewest switches surface hopping is a powerful tool to simulate nonadiabatic dynamics, both electronically and vibrationally. The details, however, matter. Correct treatment of decoherence and frustrated hops is essential for many systems. Similarly, the calculation of the diabatic population should be treated with care when diabatic couplings are large.

This review is not comprehensive of all the advances in this method. However, it is written in a format to introduce the basics and some of the subtleties of the surface hopping method to students who are beginning to work in this field. We hope that this review is helpful to both the practical users in choosing the correct implementation details and those who wish to code surface hopping for themselves for benchmarking and method development.

https://doi.org/10.1021/acsomega.2c04843
ACS Omega 2022, 7, 45810−45824

Numerically Exact Quantum Dynamics

Here we provide details of the numerically exact quantum dynamics shown in Figures 2−4. We want to numerically solve the time-dependent Schrödinger equation:

$$i\hbar\frac{\partial\Psi(q, R, t)}{\partial t} = H\Psi(q, R, t) \tag{35}$$

where $\Psi(q, R, t)$ is the total wave function, and H is the total Hamiltonian. For a time-independent Hamiltonian, the solution to eq 35 is

$$\Psi(q, R, t) = \sum_k c_k e^{-iE_k t/\hbar}\Phi_k(q, R) \tag{36}$$

where $\Phi_k(q, R)$ and E_k are the eigenfunctions and the eigenvalues of the total Hamiltonian: $H\Phi_k(q, R) = E_k\Phi_k(q, R)$ and $c_k = \langle\Phi_k|\Psi(t = 0)\rangle$ are the expansion coefficients of the initial wave function $\Psi(q, R, t = 0)$.

Note that eq 36 can only be used if the eigenfunctions (and energies) are known for the full Hamiltonian, which is computationally prohibitive for general systems with a large number of q and R coordinates. For a low-dimensional system defined by two diabats $|1\rangle$ and $|2\rangle$ and a single coordinate R, it becomes feasible to numerically solve for the eigenfunctions, however. We consider the Hamiltonian to be given by

$$H = \hat{T}_R + \begin{pmatrix} V_{11}(R) & V_{12}(R) \\ V_{21}(R) & V_{22}(R) \end{pmatrix} \tag{37}$$

where $\hat{T}_R = -\frac{\hbar^2}{2m}\frac{\partial^2}{\partial R^2}$ is the kinetic energy operator and $V_{ij}(R)$ are the electronic Hamiltonian terms (in the diabatic basis).

In the Python codes provided in ref 19 the Hamiltonian matrix is calculated in a discrete variable representation (DVR) basis.[80,81] This DVR basis intuitively represents position basis with finitely many basis functions. These DVR basis functions are defined over a uniformly spaced position grid: R_0, $R_0 + \Delta R$, $R_0 + 2\Delta R$, ..., R_N. In this uniform DVR basis, the matrix elements of the kinetic energy operator are given by[81]

$$T_{ll'} = \frac{\hbar^2}{2m\Delta R^2}(-1)^{l-l'}\begin{cases} \pi^2/3 & l = l' \\ 2/(l-l)'^2 & l \neq l' \end{cases} \tag{38}$$

We now define a combined diabatic basis as $|iR_l\rangle$ where $i = 1$ or 2 represents the electronic diabatic basis and $R_l = R_0 + (l - 1)\Delta R$ is the l'th element of the DVR grid. In this discrete basis the wave function is given by $|\Psi(t)\rangle = \sum_{i=1}^{2}\sum_{l=0}^{N}\Psi_i^d(R_l,t)|iR_l\rangle$, where $\Psi_i^d(R_l,t)$ are the expansion coefficients in the diabatic basis $|i\rangle$ at time t. The total Hamiltonian matrix elements in this basis are given by

$$H_{iR_l,i'R_{l'}} = T_{l,l'}\delta(i, i') + V_{i,i'}(R_l)\delta(l, l') \tag{39}$$

where $\delta(i,j) = 1$ if $i = j$ and 0 otherwise.

Figures 2−4 show the results of dynamics in the adiabatic basis $|\phi_j^{ad}(R_l)\rangle$. This adiabatic basis is an eigenfunction of the electronic Hamiltonian at a fixed R_l. Therefore, $H_{el}(R_l)|\phi_j^{ad}(R_l)\rangle = E_j^{ad}(R_l)|\phi_j^{ad}(R_l)\rangle$ with the matrix elements $H_{el}^{i,i'}(R_l) = V_{i,i'}(R_l)$ and $E_j^{ad}(R_l)$ are the adiabatic potential energy surfaces. Now the total wave function can be written in the adiabatic basis as $|\Psi(t)\rangle = \sum_{j=1}^{2}\sum_{l=0}^{N}\Psi_j^{ad}(R_l)|\phi_j^{ad}(R_l)R_l\rangle$ with

$$\Psi_j^{ad}(R_l) = \sum_{i=1}^{2}\Psi_i^d(R_l, t)\langle\phi_j^{ad}(R_l)|i\rangle \tag{40}$$

The coefficients $\Psi_j^{ad}(R_l, t)$ represent the nuclear wave functions on the adiabatic surface j at coordinate R_l at time t.

Therefore, to convert to the adiabatic basis, at each DVR grid point R_l, we diagonalize the 2 × 2 matrix with elements $V_{ii'}(R_l)$ to obtain the adiabatic coefficients $\langle i|\phi_j^{ad}(R_l)\rangle$ and the potential energy surfaces $E_j^{ad}(R_l)$. These adiabatic energy surfaces are plotted in Figure 1. The dynamics of $|\Psi(t)\rangle$ is evaluated in the diabatic basis to obtain $\Psi_i^d(R_l, t)$. Equation 40 is then used to calculate $\Psi_j^{ad}(R_l, t)$ whose absolute values are plotted in Figure 2. Finally, the electronic density matrix elements shown in Figures 3 and 4 are computed as $\rho_{j,j'}^{ad}(t) = \sum_l \Psi_j^{*ad}(R_l, t)\ \Psi_{j'}^{ad}(R_l, t)$.

In summary, the algorithm for the numerically exact quantum dynamics followed in ref 19 is

1. Define a grid with points R_1, R_2,⋯, R_N, with a uniform spacing $R_{l+1} - R_l = \Delta R$. The final results should be converged with respect to the grid spacing and limits.
2. Construct a $2N \times 2N$ Hamiltonian matrix using eq 39. Diagonalize this matrix to obtain the coefficients of the eigenfunctions in the diabatic basis $\langle iR_l|\Phi_k\rangle$ and eigenvalues E_k.
3. At each R_l, calculate $\langle i|\phi_j^{ad}(R_l)\rangle$ by diagonalizing the 2 × 2 matrix with elements $V_{ii'}(R_l)$.
4. Initialize $\Psi_i^d(R_l, t = 0)$ and calculate $c_k = \sum_{i,l}\Psi_i^d(R_l, t = 0)\langle\Phi_k|iR_l\rangle$.
5. Calculate $\Psi_i^d(R_l, t) = \sum_k c_k e^{-iE_k t/\hbar}\langle iR_l|\Phi_k\rangle$.
6. Calculate $\Psi_j^{ad}(R_l, t)$ using eq 40 and the electronic density matrix as $\rho_{j,j'}^{ad}(t) = \sum_l \Psi_j^{*ad}(R_l, t)\Psi_{j'}^{ad}(R_l, t)$.

The results in this work are calculated with 501 DVR points uniformly distributed from −25 au to 25 au. This gives a Hamiltonian matrix of size 1002 × 1002. This matrix is diagonalized using an inbuilt Python library.

AUTHOR INFORMATION

Corresponding Author

Amber Jain − *Department of Chemistry, Indian Institute of Technology Bombay, Mumbai 400076, India;* orcid.org/0000-0003-4108-9112; Email: amberj@chem.iitb.ac.in

Author

Aarti Sindhu − *Department of Chemistry, Indian Institute of Technology Bombay, Mumbai 400076, India;* orcid.org/0000-0003-2698-4418

Complete contact information is available at: https://pubs.acs.org/10.1021/acsomega.2c04843

Notes

The authors declare no competing financial interest.

ACKNOWLEDGMENTS

We acknowledge support from Science and Engineering Research Board, early career research award Grant no. ECR/2018/001635/CS. A.J. thanks Joe Subotnik for many insightful discussions over several years.

REFERENCES

(1) Tully, J. C. Molecular dynamics with electronic transitions. *J. Chem. Phys.* **1990**, *93*, 1061−1071.

(2) Chapman, S. The classical trajectory-surface-hopping approach to charge-transfer processes. *Adv. Chem. Phys.* **1992**, *82*, 423−483.

(3) Tully, J. C.*Modern methods for multidimensional dynamics computations in chemistry*; World Scientific, 1998; pp 34−72.

https://doi.org/10.1021/acsomega.2c04843
ACS Omega 2022, 7, 45810−45824

(4) Jasper, A. W.; Truhlar, D. G. Non-Born-Oppenheimer molecular dynamics for conical intersections, avoided crossings, and weak interactions. *Conical Intersections: Theory, Computation, and Experiment* **2011**, *17*, 375−414.
(5) Subotnik, J. E.; Jain, A.; Landry, B.; Petit, A.; Ouyang, W.; Bellonzi, N. Understanding the surface hopping view of electronic transitions and decoherence. *Annu. Rev. Phys. Chem.* **2016**, *67*, 387−417.
(6) Doltsinis, N. L. Molecular dynamics beyond the Born-Oppenheimer approximation: mixed quantum-classical approaches. *NIC Series* **2006**, *31*, 389−409.
(7) Barbatti, M. Nonadiabatic dynamics with trajectory surface hopping method. *WIREs: Comp.Mol. Sci.* **2011**, *1*, 620−633.
(8) Drukker, K. Basics of surface hopping in mixed quantum/classical simulations. *J. Chem. Phys.* **1999**, *153*, 225−272.
(9) Wang, L.; Akimov, A.; Prezhdo, O. V. Recent progress in surface hopping: 2011−2015. *J. Phys. Chem. Lett.* **2016**, *7*, 2100−2112.
(10) Malhado, J. P.; Bearpark, M. J.; Hynes, J. T. Non-adiabatic dynamics close to conical intersections and the surface hopping perspective. *Front. Chem.* **2014**, *2*, 97.
(11) Mai, S.; Richter, M.; Heindl, M.; Menger, M. F. S. J.; Atkins, A.; Ruckenbauer, M.; Plasser, F.; Ibele, L. M.; Kropf, S.; Oppel, M.; Marquetand, P.; Gonzalez, L.SHARC2.1: Surface Hopping Including Arbitrary CouplingsProgram Package for Non-Adiabatic Dynamics, 2019. sharc-md.org.
(12) Du, L.; Lan, Z. An on-the-fly surface-hopping program jade for nonadiabatic molecular dynamics of polyatomic systems: implementation and applications. *J. Chem. Theory Comput.* **2015**, *11*, 1360−1374.
(13) Barbatti, M.; Ruckenbauer, M.; Plasser, F.; Pittner, J.; Granucci, G.; Persico, M.; Lischka, H. Newton-X: a surface-hopping program for nonadiabatic molecular dynamics. *WIREs: Comput. Mol. Sci.* **2014**, *4*, 26−33.
(14) Akimov, A. V.; Prezhdo, O. V. The PYXAID program for non-adiabatic molecular dynamics in condensed matter systems. *J. Chem. Theory Comput.* **2013**, *9*, 4959−4972.
(15) Akimov, A. V. Libra: an open-source "methodology discovery" library for quantum and classical dynamics simulations. *J. Comput. Chem.* **2016**, *37*, 1626−1649.
(16) Zheng, J.; Li, Z. H.; Jasper, A. W.; Bonhommeau, D. A.; Valero, R.; Meana-Paneda, R.; Mielke, S. L.; Zhang, L.; Truhlar, D. G.*ANT*, version 2019; University of Minnesota: Minneapolis, 2019. http://comp.chem.umn.edu/ant.
(17) Shao, Y.; Gan, Z.; Epifanovsky, E.; Gilbert, A. T.; Wormit, M.; Kussmann, J.; Lange, A. W.; Behn, A.; Deng, J.; Feng, X.; et al. Advances in molecular quantum chemistry contained in the Q-Chem 4 program package. *Mol. Phys.* **2015**, *113*, 184−215.
(18) Python implementation of FSSH algorithm: https://zenodo.org/badge/latestdoi/519432030.
(19) Python implementation of numerically exact quantum dynamics: https://zenodo.org/badge/latestdoi/519436839.
(20) Fang, J.-Y.; Hammes-Schiffer, S. Improvement of the internal consistency in trajectory surface hopping. *J. Phys. Chem. A* **1999**, *103*, 9399−9407.
(21) Granucci, G.; Persico, M. Critical appraisal of the fewest switches algorithm for surface hopping. *J. Chem. Phys.* **2007**, *126*, 134114.
(22) Jain, A.; Subotnik, J. E. Does nonadiabatic transition state theory make sense without decoherence? *J. Phys. Chem. Lett.* **2015**, *6*, 4809−4814.
(23) Landry, B. R.; Subotnik, J. E. How to recover Marcus theory with fewest switches surface hopping: Add just a touch of decoherence. *J. Chem. Phys.* **2012**, *137*, 22A513.
(24) Fortran implementation of AFSSH algorithm (with decoherence): https://zenodo.org/badge/latestdoi/189350184.
(25) Jain, A.; Alguire, E.; Subotnik, J. E. An efficient, augmented surface hopping algorithm that includes decoherence for use in large-scale simulations. *J. Chem. Theory Comput.* **2016**, *12*, 5256−5268.
(26) Tanimura, Y.; Kubo, R. Time evolution of a quantum system in contact with a nearly Gaussian-Markoffian noise bath. *J. Phys. Soc. Jpn.* **1989**, *58*, 101−114.
(27) Yan, Y.-a.; Yang, F.; Liu, Y.; Shao, J. Hierarchical approach based on stochastic decoupling to dissipative systems. *Chem. Phys. Lett.* **2004**, *395*, 216−221.
(28) Ishizaki, A.; Fleming, G. R. Unified treatment of quantum coherent and incoherent hopping dynamics in electronic energy transfer: Reduced hierarchy equation approach. *J. Chem. Phys.* **2009**, *130*, 234111.
(29) Temen, S.; Jain, A.; Akimov, A. V. Hierarchical equations of motion in the Libra software package. *Int. J. Quantum Chem.* **2020**, *120*, e26373.
(30) Jain, A.; Subotnik, J. E. Surface hopping, transition state theory, and decoherence. II. Thermal rate constants and detailed balance. *J. Chem. Phys.* **2015**, *143*, 134107.
(31) Hammes-Schiffer, S.; Tully, J. C. Proton transfer in solution: Molecular dynamics with quantum transitions. *J. Chem. Phys.* **1994**, *101*, 4657−4667.
(32) Fang, J.-Y.; Hammes-Schiffer, S. Comparison of surface hopping and mean field approaches for model proton transfer reactions. *J. Chem. Phys.* **1999**, *110*, 11166−11175.
(33) Heller, E. J. Frozen Gaussians: A very simple semiclassical approximation. *J. Chem. Phys.* **1981**, *75*, 2923−2931.
(34) Bittner, E. R.; Rossky, P. J. Quantum decoherence in mixed quantum-classical systems: Nonadiabatic processes. *J. Chem. Phys.* **1995**, *103*, 8130−8143.
(35) Schwartz, B. J.; Bittner, E. R.; Prezhdo, O. V.; Rossky, P. J. Quantum decoherence and the isotope effect in condensed phase nonadiabatic molecular dynamics simulations. *J. Chem. Phys.* **1996**, *104*, 5942−5955.
(36) Prezhdo, O. V.; Rossky, P. J. Evaluation of quantum transition rates from quantum-classical molecular dynamics simulations. *J. Chem. Phys.* **1997**, *107*, 5863−5878.
(37) Volobuev, Y. L.; Hack, M. D.; Topaler, M. S.; Truhlar, D. G. Continuous surface switching: An improved time-dependent self-consistent-field method for nonadiabatic dynamics. *J. Chem. Phys.* **2000**, *112*, 9716−9726.
(38) Wong, K. F.; Rossky, P. J. Solvent-induced electronic decoherence: Configuration dependent dissipative evolution for solvated electron systems. *J. Chem. Phys.* **2002**, *116*, 8429−8438.
(39) Bedard-Hearn, M. J.; Larsen, R. E.; Schwartz, B. J. Mean-field dynamics with stochastic decoherence (MF-SD): A new algorithm for nonadiabatic mixed quantum/classical molecular-dynamics simulations with nuclear-induced decoherence. *J. Chem. Phys.* **2005**, *123*, 234106.
(40) Zhu, C.; Nangia, S.; Jasper, A. W.; Truhlar, D. G. Coherent switching with decay of mixing: an improved treatment of electronic coherence for non-Born-Oppenheimer trajectories. *J. Chem. Phys.* **2004**, *121*, 7658−7670.
(41) Zhu, C.; Jasper, A. W.; Truhlar, D. G. Non-Born-Oppenheimer Liouville-von Neumann dynamics. Evolution of a subsystem controlled by linear and population-driven decay of mixing with decoherent and coherent switching. *J. Chem. Theory Comput.* **2005**, *1*, 527−540.
(42) Granucci, G.; Persico, M.; Zoccante, A. Including quantum decoherence in surface hopping. *J. Chem. Phys.* **2010**, *133*, 134111.
(43) Jasper, A. W.; Truhlar, D. G. Electronic decoherence time for non-Born-Oppenheimer trajectories. *J. Chem. Phys.* **2005**, *123*, 064103.
(44) Subotnik, J. E.; Ouyang, W.; Landry, B. R. Can we derive Tully's surface-hopping algorithm from the semiclassical quantum Liouville equation? Almost, but only with decoherence. *J. Chem. Phys.* **2013**, *139*, 214107.
(45) Horenko, I.; Salzmann, C.; Schmidt, B.; Schütte, C. Quantum-classical Liouville approach to molecular dynamics: Surface hopping Gaussian phase-space packets. *J. Chem. Phys.* **2002**, *117*, 11075−11088.

https://doi.org/10.1021/acsomega.2c04843
ACS Omega 2022, 7, 45810−45824

(46) Landry, B. R.; Falk, M. J.; Subotnik, J. E. Communication: The correct interpretation of surface hopping trajectories: How to calculate electronic properties. *J. Chem. Phys.* **2013**, *139*, 211101.
(47) Nitzan, A.*Chemical dynamics in condensed phases: relaxation, transfer and reactions in condensed molecular systems*; Oxford University Press, 2006.
(48) Adolphs, J.; Renger, T. How proteins trigger excitation energy transfer in the FMO complex of green sulfur bacteria. *Biophys. J.* **2006**, *91*, 2778−2797.
(49) Sindhu, A.; Jain, A. Benchmarking the Surface Hopping Method to Include Nuclear Quantum Effects. *J. Chem. Theory Comput.* **2021**, *17*, 655−665.
(50) Parandekar, P. V.; Tully, J. C. Mixed quantum-classical equilibrium. *J. Chem. Phys.* **2005**, *122*, 094102.
(51) Jasper, A. W.; Hack, M. D.; Truhlar, D. G. The treatment of classically forbidden electronic transitions in semiclassical trajectory surface hopping calculations. *J. Chem. Phys.* **2001**, *115*, 1804−1816.
(52) Jasper, A. W.; Stechmann, S. N.; Truhlar, D. G. Fewest-switches with time uncertainty: A modified trajectory surface-hopping algorithm with better accuracy for classically forbidden electronic transitions. *J. Chem. Phys.* **2002**, *116*, 5424−5431.
(53) Jasper, A. W.; Truhlar, D. G. Improved treatment of momentum at classically forbidden electronic transitions in trajectory surface hopping calculations. *Chem. Phys. Lett.* **2003**, *369*, 60−67.
(54) Jain, A.; Herman, M. F.; Ouyang, W.; Subotnik, J. E. Surface hopping, transition state theory and decoherence. I. Scattering theory and time-reversibility. *J. Chem. Phys.* **2015**, *143*, 134106.
(55) Carof, A.; Giannini, S.; Blumberger, J. Detailed balance, internal consistency, and energy conservation in fragment orbital-based surface hopping. *J. Chem. Phys.* **2017**, *147*, 214113.
(56) Nelson, T.; Fernandez-Alberti, S.; Roitberg, A. E.; Tretiak, S. Nonadiabatic excited-state molecular dynamics: Treatment of electronic decoherence. *J. Chem. Phys.* **2013**, *138*, 224111.
(57) Tully, J. C. Mixed quantum-classical dynamics. *Faraday Discuss.* **1998**, *110*, 407−419.
(58) Subotnik, J. E.; Rhee, Y. M. On surface hopping and time-reversal. *J. Phys. Chem. A* **2015**, *119*, 990−995.
(59) Tolman, R. C.*The principles of statistical mechanics*; Courier Corporation, 1979.
(60) Mahan, B. H. Microscopic reversibility and detailed balance. an analysis. *J. Chem. Educ.* **1975**, *52*, 299.
(61) Schmidt, J.; Parandekar, P. V.; Tully, J. C. Mixed quantum-classical equilibrium: Surface hopping. *J. Chem. Phys.* **2008**, *129*, 044104.
(62) Sherman, M.; Corcelli, S. Thermal equilibrium properties of surface hopping with an implicit Langevin bath. *J. Chem. Phys.* **2015**, *142*, 024110.
(63) Sifain, A. E.; Wang, L.; Prezhdo, O. V. Communication: Proper treatment of classically forbidden electronic transitions significantly improves detailed balance in surface hopping. *J. Chem. Phys.* **2016**, *144*, 211102.
(64) Smith, B.; Akimov, A. V. A comparative analysis of surface hopping acceptance and decoherence algorithms within the neglect of back-reaction approximation. *J. Chem. Phys.* **2019**, *151*, 124107.
(65) Fang, J.-Y.; Hammes-Schiffer, S. Nonadiabatic dynamics for processes involving multiple avoided curve crossings: Double proton transfer and proton-coupled electron transfer reactions. *J. Chem. Phys.* **1997**, *107*, 8933−8939.
(66) Morelli, J.; Hammes-Schiffer, S. Surface hopping and fully quantum dynamical wavepacket propagation on multiple coupled adiabatic potential surfaces for proton transfer reactions. *Chem. Phys. Lett.* **1997**, *269*, 161−170.
(67) Hazra, A.; Soudackov, A. V.; Hammes-Schiffer, S. Isotope effects on the nonequilibrium dynamics of ultrafast photoinduced proton-coupled electron transfer reactions in solution. *J. Phys. Chem. Lett.* **2011**, *2*, 36−40.
(68) Goyal, P.; Schwerdtfeger, C. A.; Soudackov, A. V.; Hammes-Schiffer, S. Proton quantization and vibrational relaxation in nonadiabatic dynamics of photoinduced proton-coupled electron transfer in a solvated phenol-amine complex. *J. Phys. Chem. B* **2016**, *120*, 2407−2417.
(69) Jain, A.; Subotnik, J. E. Vibrational Energy Relaxation: A Benchmark for Mixed Quantum-Classical Methods. *J. Phys. Chem. A* **2018**, *122*, 16−27.
(70) Käb, G. Fewest switches adiabatic surface hopping as applied to vibrational energy relaxation. *J. Phys. Chem. A* **2006**, *110*, 3197−3215.
(71) A-FSSH Fortran codes with decoherence and explicit vibrational quantization: https://zenodo.org/badge/latestdoi/498033787.
(72) Meek, G. A.; Levine, B. G. Evaluation of the time-derivative coupling for accurate electronic state transition probabilities from numerical simulations. *J. Phys. Chem. Lett.* **2014**, *5*, 2351−2356.
(73) Min, S. K.; Agostini, F.; Tavernelli, I.; Gross, E. K. Ab initio nonadiabatic dynamics with coupled trajectories: A rigorous approach to quantum (de) coherence. *J. Phys. Chem. Lett.* **2017**, *8*, 3048−3055.
(74) Ben-Nun, M.; Quenneville, J.; Martínez, T. J. Ab initio multiple spawning: Photochemistry from first principles quantum molecular dynamics. *J. Phys. Chem. A* **2000**, *104*, 5161−5175.
(75) Makri, N. Numerical path integral techniques for long time dynamics of quantum dissipative systems. *J. Chem. Phys.* **1995**, *36*, 2430−2457.
(76) Petit, A. S.; Subotnik, J. E. Appraisal of surface hopping as a tool for modeling condensed phase linear absorption spectra. *J. Chem. Theory Comput.* **2015**, *11*, 4328−4341.
(77) Miao, G.; Subotnik, J. Revisiting the recoherence problem in the fewest switches surface hopping algorithm. *J. Phys. Chem. A* **2019**, *123*, 5428−5435.
(78) Kelly, A.; Markland, T. E. Efficient and accurate surface hopping for long time nonadiabatic quantum dynamics. *J. Chem. Phys.* **2013**, *139*, 014104.
(79) Dral, P. O.; Barbatti, M.; Thiel, W. Nonadiabatic excited-state dynamics with machine learning. *J. Phys. Chem. Lett.* **2018**, *9*, 5660−5663.
(80) Lill, J.; Parker, G.; Light, J. Discrete variable representations and sudden models in quantum scattering theory. *Chem. Phys. Lett.* **1982**, *89*, 483−489.
(81) Colbert, D. T.; Miller, W. H. A novel discrete variable representation for quantum mechanical reactive scattering via the S-matrix Kohn method. *J. Chem. Phys.* **1992**, *96*, 1982−1991.

https://doi.org/10.1021/acsomega.2c04843
ACS Omega 2022, 7, 45810−45824